High-throughput Exploration of the Network Dependent on AKT1 in Mouse Ovarian Granulosa Cells

Authors

Maëva Elzaiat, Laetitia Herman, Bérangère Legois, Thibaut Léger, Anne-Laure Todeschini, and Reiner A. Veitia

Correspondence

reiner.veitia@ijm.fr,
anne-laure.todeschini@ijm.fr

In Brief

The PI3K/AKT signaling pathway is known to regulate a broad range of cellular processes, and it is often altered in cancer. We have performed high-throughput analyses of the proteins and transcripts deregulated after *Akt1* depletion in primary murine granulosa cells, which are the supporting cells of the oocyte. We found known and novel cellular processes perturbed by *AKT1* knock-down. Our results confirm and extend the role of this kinase in critical cellular processes, such as directional migration, and provide a series of new substrate candidates that deserve further investigation.

Graphical Abstract

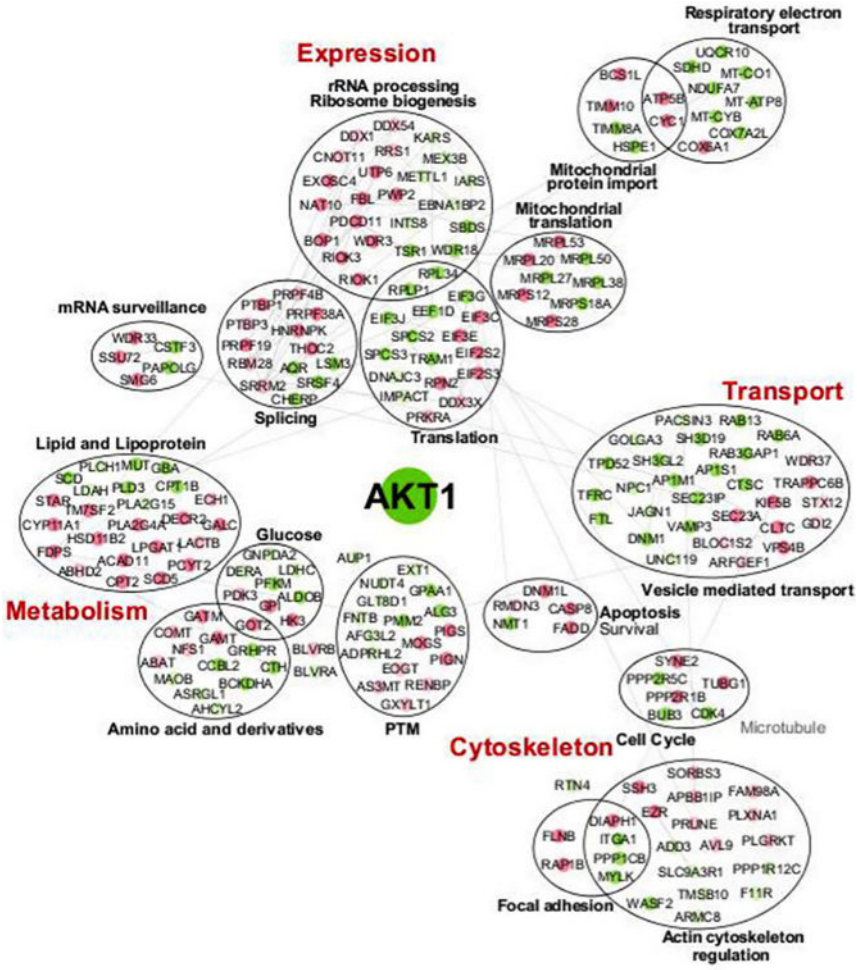

Network dependent on AKT1 in murine granulosa cells

Highlights

- Proteome and transcriptome analysis after Akt1 KD in mouse primary granulosa cells.
- A resource of known and novel biological processes regulated by AKT1.
- A resource of putative kinases and transcription factors acting downstream of AKT1.
- Altered velocity and directional migration in granulosa cells depleted for Akt1.

Elzaiat et al., 2019, Molecular & Cellular Proteomics *18*, 1307–1319

https://doi.org/10.1074/mcp.RA119.001461

High-throughput Exploration of the Network Dependent on AKT1 in Mouse Ovarian Granulosa Cells*[S]

Maëva Elzaiat‡§, Laetitia Herman‡§, Bérangère Legois‡§, Thibaut Léger‡, Anne-Laure Todeschini‡§‖, and Reiner A. Veitia‡§¶

The PI3K/AKT signaling pathway is known to regulate a broad range of cellular processes, and it is often altered in several types of cancers. Recently, somatic *AKT1* mutations leading to a strong activation of this kinase have been reported in juvenile granulosa cell tumors. However, the molecular role of AKT1 in the supporting cell lineage of the ovary is still poorly understood. To get insights into its function in such cells, we depleted *Akt1* in murine primary granulosa cells and assessed the molecular consequences at both the transcript and protein levels. We were able to corroborate the involvement of AKT1 in the regulation of metabolism, apoptosis, cell cycle, or cytoskeleton dynamics in this ovarian cell type. Consistently, we showed in established granulosa cells that depletion of *Akt1* provoked altered directional persistent migration and increased its velocity. This study also allowed us to put forward new direct and indirect targets of the kinase. Indeed, a series of proteins involved in intracellular transport and mitochondrial physiology were significantly affected by *Akt1* depletion. Using *in silico* analyses, we also propose a set of kinases and transcription factors that can mediate the action of AKT1 on the deregulated transcripts and proteins. Taken altogether, our results provide a resource of direct and indirect AKT1 targets in granulosa cells and may help understand its roles in this ovarian cell type. ***Molecular & Cellular Proteomics 18: 1307–1319, 2019. DOI: 10.1074/mcp.RA119.001461.***

The AKT/PKB[1] is the major downstream effector of the PI3K signaling pathway known to regulate a broad range of cellular functions such as: survival, proliferation, growth, metabolism, and migration (reviewed in (1, 2). The AKT family comprises three widely expressed members, namely, AKT1/PKBα, AKT2/PKBβ, and AKT3/PKBγ. However, the study of paralog-specific knockout mice have shown both redundant and distinct roles for the three *AKT* genes (3, 4). The prototypic AKT protein is highly conserved and contains three domains: an N terminus PHD, a central kinase domain, and a C terminus regulatory domain containing a hydrophobic motif. Activation of the PI3K by different cytokines and growth factors leads to the production of PIP2/PIP3 (1). AKT interacts with membrane PIP3 thanks to its PHD. The protein kinase is thus transiently relocalized to the plasma membrane where it is phosphorylated by the phosphoinositide-dependent protein kinase 1 on Thr308 and by mammalian target of rapamycin complex (mTORC) 2 on Ser473, leading to its full activation (5, 6).

A number of AKT downstream target substrates have been described (1, 2, 7). For example, AKT promotes cell survival via the phosphorylation of proapoptotic factors like BCL2 associated agonist of cell death (8) or via the activation of the E3 ubiquitin ligase mouse double minute 2 homolog (9). Besides, it exerts genomic effects by modulating the activity of various TFs. For instance, by inhibiting the phosphorylation of forkhead box O factors, which leads to their export from the nucleus, AKT regulates cell survival, thus blocking the transcription of proapoptotic genes such as *BCL2 like 11* or *fas ligand* (10–12). It is also known to activate CREB1 and nuclear factor kappa B subunit (NFκB) to promote cell survival (13, 14). Furthermore, AKT stimulates cell proliferation by inhibiting inhibitors of cell-cycle progression, like p27 (15) or by stabilizing proteins involved in cell-cycle entry by phosphorylation of their inhibitor, namely, the glycogen synthase kinase 3 (16). Another well-documented function of AKT is its role in promoting cell growth, which is achieved via the regulation of mTORC1, a critical regulator of translation initiation and ribosome biogenesis (17). AKT regulates nutrient uptake by regulating the localization of glucose transporter type 4 at the plasma membrane (18, 19) and promotes energy storage by inhibiting glycogen synthase kinase 3 (20). Angiogenesis and vascular remodeling are stimulated by the positive regulation of endothelial nitric oxide synthase by AKT in endothelial cells (21). Finally, AKT fosters cell migration and invasion, notably via the regulation of the actin cytoskeleton (22–24) and the secretion of matrix metalloproteases (25).

As a consequence of its central position in the physiology of the cell, AKT dysregulation is associated with several human diseases, including cancer. Indeed, many human cancers

From the ‡Institut Jacques Monod, Université Paris-Diderot, 75013 Paris, France; §Université Paris-Diderot, 75013 Paris, France
Received March 21, 2019
Published, MCP Papers in Press, April 16, 2019, DOI 10.1074/mcp.RA119.001461

show elevated activity of AKT (reviewed in (26)). This hyperactivity can result from mutations in genes encoding upstream regulators of AKT, like *PI3K* (27) or *phosphatase* and *TENsin homolog* (28) and by rare mutations directly affecting *AKT* (29, 30). The most frequently reported *AKT* mutation, E17K, affects its PHD and results in an increased activity and a localization of to the plasma membrane (31). Point mutations of AKT are found spread all along the coding sequence (cBioPortal, http://www.cbioportal.org/). However, due to their low frequency, their status of drivers of tumorigenesis is not clear. Recently, we identified mutations affecting *AKT1* as a hallmark of juvenile granulosa cell tumors. Indeed, we found that more than 60% of the tumor samples studied bore somatic in-frame tandem duplications affecting the PHD of AKT1 whereas the others carried potentially damaging point mutations at conserved residues (32). Remarkably, the AKT1 variants bearing the tandem duplications were insensitive to serum deprivation, they were constitutively hyper-phosphorylated, and this was associated with hyperactivity and relocalization to the plasma membrane (32). Importantly, the mutational analysis of four juvenile granulosa cell tumor samples bearing AKT1 tandem duplications by RNA sequencing showed that these insertions were the sole detectable lesions common to the four tumors (33), strongly suggesting that they constitute the driving event in these tumors. However, little is known about the role of AKT1 in granulosa cells at the molecular level. To date, only scarce data from studies performed in mouse knock-out models are available. *Akt1*$^{-/-}$ female mice show reduced fertility due to altered follicular development and abnormal oocyte growth (34). In the *Akt1*$^{-/-}$ ovaries, expression of cell-cycle positive regulators *Cyclin D1* and *Cyclin D3* are reduced as well as the expression of the anti-apoptotic factor *BCL2 like 1* and of the survival factor *KIT ligand* (34). No molecular analyses have been performed, particularly, in healthy granulosa cells that could help understand the pathophysiological roles of AKT.

In this study, we have performed high-throughput analyses of the proteins and transcripts deregulated after *Akt1* depletion in mouse pGCs, which are the supporting cells of germ cell development and function (35). We found multiple cellular processes perturbed by the *AKT1* KD, such as cytoskeleton regulation and focal adhesion. Consistently, we found that granulosa cells depleted for *Akt1* displayed an altered directional persistent migration. Taken together, our transcriptomic and proteomic data can help understand the role of AKT1 in this critical ovarian cell type.

EXPERIMENTAL PROCEDURES

Cell Culture—Murine primary granulosa cells were collected from ovaries of 8-week-old female Swiss mice (Janvier Labs, Le Genest Saint Isle, France) and cultured as described in (36). The cell line AT29C derived from a mouse ovarian tumor was kindly provided by Dr. N. Di Clemente and cultured in DMEM supplemented with 10% FBS and 1% penicillin-streptomycin (Thermo Fisher Scientific, Waltham, Massachusetts) (37).

Transfection and Reagents—Cells were transiently transfected in six-well plates with 30 pmoles of a pool of three different siRNAs against *Akt1* (Dharmacon, Lafayette, Colorado; ON-TARGETplus siRNAs, pool KD1: J-040709-06-0005, J-040709-07-0005, J-040709-08-0005, KD2: J-040709-06-0005, J-040709-08-0005, J-040709-09-0005, KD3: J-040709-06-0005, J-040709-07-0005, J-040709-09-0005, and KD4: J-040709-07-0005, J-040709-08-0005, J-040709-09-0005) or 100 pmoles of a pool of two different siRNAs against *Creb1* (Sigma-Aldrich, St. Louis, Missouri, SASI_Mm01_00191782 and SASI_Mm01_00191783), *Nfkb2* (Sigma-Aldrich, SASI_Mm01_00151272 and SASI_Mm01_00151273), or *Wt1* (Sigma-Aldrich, SASI_Mm01_00101396 and SASI_Mm01_00101398) or an equal amount of the nontargeting/scrambled siRNA (Dharmacon, D-001810-10-05) using Lipofectamine RNAiMax (Thermo Fisher Scientific). 5 h after transfection, the mix was replaced by culture

[1] The abbreviations used are: AKT, AKT serine/threonine protein kinase; 4E-BP1, eukaryotic translation initiation factor 4E binding protein 1; ASCC1, activating signal cointegrator 1 complex subunit 1; BRD8, bromodomain containing 8; CALM1, calmodulin 1; Capn1, calpain 1; CBX1, chromobox 1; Cdhr1, cadherin-related family member 1; CEBPB, CCAAT enhancer binding protein beta; CREB1, cAMP-responsive element-binding protein 1; Crip1, cysteine-rich protein 1; CTBP1, C-terminal binding protein 1; DDX1, DEAD-box helicase 1; DDX3X, DEAD-box helicase 3 X-linked; DDX54, DEAD-box helicase 54; DEProts, proteins differentially expressed; DHX36, DEAH-box helicase 36; DPhospho, proteins differentially phosphorylated; Ecm1, extracellular matrix protein 1; EEF1D, eukaryotic translation elongation factor 1 delta; EIF2S2, eukaryotic translation initiation factor 2 subunit beta; ELP4, elongator acetyltransferase complex subunit 4; EMX2, empty spiracles homeobox 2; ENY2, transcription and export complex 2 subunit; Eri3, ERI1 exoribonuclease family member 3; FOXP1, forkhead box P1; GATA4, GATA-binding protein 4; GOT2, glutamic-oxaloacetic transaminase 2; GTF2E2, general transcription factor IIE subunit 2; HMGB2, high mobility group box 2; HNRNPK, heterogeneous nuclear ribonucleoprotein K; HSF1, heat shock transcription factor 1; KD, knock(ed)-down; Log2FC, log2fold change; MECP2, methyl-CpG-binding protein 2; MED23, mediator complex subunit 23; MED4, mediator complex subunit 4; MS, mass spectrometry; mTORC1, mammalian target of rapamycin complex 1; mTORC2, mammalian target of rapamycin complex 2; Mvd, mevalonate diphosphate decarboxylase; NFE2L2, nuclear factor, erythroid 2 like 2; NFκB, nuclear factor kappa B subunit; Ovgp1, oviductal glycoprotein 1; Pdlim7, PDZ and LIM domain 7; PELP1, proline-, glutamate-, and leucine-rich protein 1; pGCs, mouse primary granulosa cells; PHD, pleckstrin homology domain; PHF6, PHD finger protein 6; PI3K, phosphoinositide3-kinase; PIP2/PIP3, phosphatidylinositol-di/trisphosphate; PIR, pirin; PKB, protein kinase B; PPI, protein-protein interactions; Ppib, peptidylprolyl isomerase B; PTM, posttranslational modifications; PTMA, prothymosin alpha; RBPMS, RNA-binding protein, MRNA-processing factor; RNAi, RNA interference; RNA-seq, RNA-sequencing; RNF2, ring finger protein 2; RTN4, reticulon 4; S100a16, S100 calcium-binding protein A16; S6K1/2, ribosomal protein S6 kinase B1/B2; SFR1, SWI5 dependent homologous recombination repair protein 1; Smarca2, SWI/SNF-related, matrix-associated, actin-dependent regulator of chromatin, subfamily A, member 2; SRRM2, serine/arginine repetitive matrix 2; TCOF1, treacle ribosome biogenesis factor 1; TFAM, transcription factor A, mitochondrial; TFAP2C, transcription factor AP-2 gamma; TFs, transcription factors; TLE4, transducing-like enhancer of split 4; Tmem109, transmembrane protein 109; TSC1, tuberous sclerosis 1 protein; TSC2, tuberous sclerosis 2 protein; WT1, Wilms tumor 1; ZBED6, zinc finger BED-type containing 6.

medium, and cells were allowed to grow for 25 h before performing subsequent experiments.

RNA Extraction and Sequencing—RNA extraction was performed 30 h after transfection, following the acid guanidinium thiocyanate-phenol-chloroform (TRI)–reagent supplier's instructions (Molecular Research Center, Cincinnati, Ohio). 1.3 μg of total RNAs underwent high throughput sequencing at the IMAGIF platform (https://www.i2bc.paris-saclay.fr/, Gif-sur-Yvette, France). Specifically, total RNA quality was assessed on an Agilent Bioanalyzer 2100, using RNA 6000 pico kit (Agilent Technologies, Santa Clara, California). Directional RNA-Seq Libraries were constructed using the TruSeq mRNA Stranded library prep kit (Illumina, San Diego, California), following the manufacturer's instructions. Final library quality was assessed on an Agilent Bioanalyzer 2100, using an Agilent High Sensitivity DNA Kit. Libraries were pooled in equimolar proportions and sequenced on Single Read 75 pb runs, on an Illumina NextSeq500 instrument, using NextSeq 500 High Output 75 cycles kits. Demultiplexing was performed using bcl2fastq2 V2.15.0 and adapters were removed with Cutadapt1.9.1. Only reads longer than 10 pb were kept for analysis (about 10,000,000 reads per sample). Reads were mapped on the mouse genome (MM10) with TopHat2. Mapped reads were assigned to features with *features count* (1.5.0-p2).

RT-qPCR—The KD efficiencies were evaluated by RT-qPCR. RNA extraction was performed after 30 h of transfection. cDNA synthesis was performed with 1 μg of total RNAs after DNase treatment (New England Biolabs, Evry, France), using the M-MLV RT enzyme according to the manufacturer's protocol (Thermo Fisher Scientific). RT-qPCR was performed using the GoTaq qPCR Master Mix 5X (Promega, Madison, Wisconsin) in the Stratagene Mx3000P qPCR System. The primers used for each gene of interest are listed in Supplemental Table S9, *Sdha* served as the reference gene. The results were analyzed and presented with Excel® (Microsoft, Redmond, Washington).

Western Blots—The KD efficiency was confirmed by Western blotting. Whole cell lysates were obtained using radioimmune precipitation assay buffer (50 mM Tris-HCl, pH 8.0, with 150 mM sodium chloride, 1.0% Igepal CA-630 (NP-40), 0.5% sodium deoxycholate, and 0.1% sodium dodecyl sulfate) 30 h after transfection. Lysates were sonicated for 10 min then cleared by centrifugation, and supernatants were kept for Bradford dosage. Protein extracts (20 μg) were denatured 5 min at 96 °C in NuPAGE LDS Sample Buffer 4X (Invitrogen, Carlsbad, California) containing 5% β-mercaptoethanol. Samples were loaded on a NuPAGE Novex 4–12% Bis-Tris Gel (Invitrogen) then transferred to a polyvinylidene difluoride membrane using the standard protocol of the iBlot2 Gel Transfer device (Invitrogen). After 1 h incubation with 5% nonfat milk in phosphate-buffered saline–1% Tween (PBS-T), the membrane was incubated with antibodies against AKT1/2/3 (H-136) (1:200, Santa Cruz Biotechnology, Dallas, Texas; #sc-8312), CREB1 (D-12) (1:200, Santa Cruz Biotechnology, #sc-377154), NFκB2 (1:2 000, Abcam, Cambridge, UK, #ab109440), or glyceraldehyde-3-phosphate dehydrogenase (GAPDH) (1:1,000, Applied Biological Materials, Richmond, Canada; #G041) overnight at 4 °C. Membranes were then washed three times for 10 min and incubated with a 1:20,000 dilution of horseradish peroxidase-conjugated anti-rabbit (Jackson ImmunoResearch Laboratories, Cambridgeshire, UK; #111-035-003) or anti-mouse (Jackson ImmunoResearch Laboratories, # 115-035-003) antibodies for 1 h 30 min. Blots were finally washed three times with PBS-T and revelation was performed with the SuperSignal WEST PICO Chemiluminescent Substrate (Pierce) according to the manufacturer's protocol. Acquisitions were realized using the ImageQuant LAS4000 software on the LAS4000 device (GE Healthcare, Chicago, Illinois). Bands intensity quantification and normalization of was performed with Fiji software (38).

Mass Spectrometry Analysis—

LC-MS/MS Acquisition—Protein extracts (30 μg) from control cells (control, three replicates), and siRNA for *Akt1* cells (KD1, KD2, K3, KD4, two replicates each) were precipitated with acetone at −20 °C during 3 h and incubated with 20 μl of 25 mM NH_4HCO_3 containing sequencing-grade trypsin (12.5 μg/ml; Promega) overnight at 37 °C. Peptides were desalted using ZipTip μ-C18 Pipette Tips (Millipore, Burlington, Massachusetts) and analyzed in a Q-Exactive Plus mass spectrometer coupled to a Nano-LC Proxeon 1000 equipped with an easy spray ion source (all from Thermo Fisher Scientific). Peptides were separated by liquid chromatography with the following parameters: Acclaim PepMap100 C18 precolumn (2 cm, 75 μm inner diameter, 3 μm, 100 Å), Pepmap-RSLC Proxeon C18 column (50 cm, 75 μm inner diameter, 2 μm, 100 Å), 300 nl/min flow rate, gradient from 95% solvent A (water, 0.1% formic acid) to 35% solvent B (100% acetonitrile, 0.1% formic acid) over a period of 98 min, followed by a regeneration column for 23 min, giving a total run time of 2 h. Peptides were analyzed in the Orbitrap cell (Thermo Fisher Scientific), in full ion scan mode, at a resolution of 70,000 (at *m/z* 200), with a mass range of *m/z* 375–1,500 and an automatic gain control target of 3×10^6. Fragments were obtained by high collision-induced dissociation activation with a collisional energy of 30%, and a quadrupole isolation window of 1.4 Da. MS/MS data were acquired in the Orbitrap cell in a Top20 mode, at a resolution of 17,500, with an automatic gain control target of 2×10^5, with a dynamic exclusion of 30 s. MS/MS of most intense precursors was first acquired. The maximum ion accumulation times were set to 50 ms for MS acquisition and 45 ms for MS/MS acquisition.

Peptide and Protein Identification and Quantification—Label-free relative quantification was performed in between subject analysis using Progenesis-Qi software 4.0 (Nonlinear Dynamics Ltd., Newcastle, UK). For the identification step, all MS and MS/MS data were processed with the Proteome Discoverer software (Thermo Scientific, version 2.1) coupled to the Mascot search engine (Matrix Science, version 2.5.1, London, UK). The mass tolerance was set to 6 ppm for precursor ions and 0.02 Da for fragments. The maximum number of missed cleavages was limited to two for the trypsin protease. The following variable modifications were allowed: oxidation (Met), phosphorylation (Ser, Thr, Tyr), acetylation (Protein N-term). The SwissProt database (02/2017, #16854) with the *Mus musculus* taxonomy was used for the MS/MS identification step. Statistical methods are developed in the "Experimental Design and Statistical Rationale" section.

In Silico Analyses—To reveal the different cellular processes affected by *Akt1* depletion, we used GeneMania (https://genemania.org/) to build a network based on the physical interactions referenced to occur among the 364 DEProts and 8 DPhospho peptides. Of the 336 proteins included in the analysis 158 were connected within the network and 178 remain isolated. For such orphan deregulated proteins, we used GeneCards database (https://www.genecards.org/) to explore their implication in any cellular process. Enrichment analyses were performed with Gene Set Enrichment Analysis database (http://software.broadinstitute.org/gsea/index.jsp). We chose to illustrate the processes having at least five proteins in the overlap with published datasets. Cytoscape was used to draw and display the network (39).

To identify the DPhospho peptides, we first plotted the values of Log2FC expression *versus* the values of Log2FC phosphorylation. To make the intercept equal to 0, we subtracted the offset of the trend line (*i.e.* 0.485) to the log2FC phosphorylation values. Next, we calculated the normalized differences between Log2FC expression (A) and corrected Log2FC phosphorylation (B) for each differentially phosphorylated peptide identified ([max(A.B) - min(A.B)]/(A + B)). Then, we detected the DPhospho peptides as the outliers using the Iglewicz and Hoaglin's test (setting the modified Z score $\geq$ 1, http://contchart.com/outliers.aspx). We used GPS3.0 (http://gps.biocuckoo.

org) and PhosphoNET (http://www.phosphonet.ca/default.aspx) as prediction tools to identify the kinases potentially involved in the phosphorylation of the phosphosite of interest. The list of known kinase substrates of AKT1 was retrieved from the PhosphoSite Plus website (https://www.phosphosite.org/homeAction). GeneMania and Cytoscape were used to draw a network.

To identify the TFs potentially implicated in the regulation of the differentially expressed mRNAs (DE-mRNAs), we submitted the list of the DE-mRNAs to EnrichR database (http://amp.pharm.mssm.edu/Enrichr/), focusing on the TF-LOF tab, which corresponds to gene expression signatures extracted from the gene expression omnibus (GEO) database for TF perturbations. We kept the TFs with nominal p value < 0.05.

Cell Migration Assays—Cell velocity was assessed by a scratch-wound assay. AT29C cells of the control and KD conditions were trypsinized 24 h after transfection. 3.5×10^5 cells were plated in 24-well plates. When cells reached confluence, a thin wound was performed by scratching the culture with a pipette tip. Acquisitions of images of wound closure were performed using the IncuCyte ZOOM live-cell analysis system (Essen BioScience, Hertfordshire, UK). Images of three fields along the diameter of the well were taken at 4X magnification with the Basler scout scA1400–30gm monochrome camera every 2 h during 12 h. The wound closure was measured as described in "Experimental Design and Statistical Rationale."

Cell directional migration was assessed by letting the cells migrate on a fibronectin pattern. First, cleaned silanized glass coverslips were coated with polydimethylsiloxane (PDMS) (40). For micropattern printing, 200-μm wide PDMS stamps were prepared by pouring a PDMS solution (Sylgard 184, Dow Corning, Midland, Michigan) and allowing it to polymerize at 60 °C overnight (41). The PDMS stamps were pulled off and incubated face up for 45 min at room temperature with fibronectin. After several washes with deionized water, the stamps were dried and applied onto silanized glass coverslips, then the printed areas were blocked with 3% BSA, 0.2% Pluronic (Thermo Fisher Scientific) for 1 h at room temperature. The silanized glass coverslips were then dropped into a six-well plate. AT29C cells of the control and KD conditions were trypsinized 24 h after transfection. 10^5 cells were plated on a small portion of the printed area delimited by a PDMS barrier so that the cells could not spread. When adherent, the PDMS barrier was removed and cell migration on a fibronectin matrix was imaged at 10X magnification with the Axiocam HRc camera (Zeiss, Oberkochen, Germany) on the Axio Observer Z.1 microscope (Zeiss), every 30 min during 24 h. Analysis was performed as described in "Experimental Design and Statistical Rationale."

Experimental Design and Statistical Rationale—For the analysis of *Akt1* KD by RNA sequencing and MS, three control samples (CTRL) and eight KD samples were provided to the corresponding platform (see previous sections). CTRL samples were derived from cells transfected with nontargeting/scrambled siRNA (Dharmacon, D-001810-10-05), and KD samples were derived from cells transfected a pool of three different siRNAs against *Akt1* (Dharmacon, ON-TARGETplus siRNAs, pool KD1: J-040709-06-0005, J-040709-07-0005, J-040709-08-0005, KD2: J-040709-06-0005, J-040709-08-0005, J-040709-09-0005, KD3: J-040709-06-0005, J-040709-07-0005, J-040709-09-0005, and KD4: J-040709-07-0005, J-040709-08-0005, J-040709-09-0005).

For RNA-sequencing, differential analysis was performed with DESeq2, comparing the three CTRL samples results to the eight KD results. The p values were adjusted for multiple testing using the Benjamini and Hochberg method, and those with an adjusted p value < 0.05 were considered to be significant.

For MS, peptide identifications were validated using a 1% false discovery rate threshold calculated with the Percolator algorithm. The ptmRS node from Proteome Discoverer 2.1 was used to provide a confidence measure of phosphorylated positions for each identified peptides. Phosphorylated peptides with a ptmRS binomial peptide score above 50 were further considered (42). Protein abundance variations were measured according to the Hi-3 label-free quantification method and validated if their analysis of variance (Anova) p values were under 0.05. However, 224 proteins were not detected in all the samples. For these cases, we kept the proteins detected in at least 2/3 of samples for the control condition and 5/8 of samples for the KD condition. Statistical significance was then evaluated by a Student's t test. By this method, we detected 18 proteins with significant uncorrected p values, among which 13 had a Log2FC > 1.5 in either direction. After a Bonferonni correction, only one protein, RPS6KA2, remained significantly differentially expressed. The MS proteomics data have been deposited to the ProteomeXchange Consortium via the PRIDE (43) partner repository with the dataset identifier PXD012548 as .raw files, Proteome Discoverer 2.1 .pdResult file, associated pep.xml and xlsx files, and label-free report generated by Progenesis QI.

For the scratch-wound assay, three independent experiments were performed, with two wells used for CTRL and KD1 condition at each experiment. The wound closure was measured by calculating the decrease of the wound area over time with respect to the initial area ($area_t/area_{t0}$) using Fiji software. The slope of the line generated in the two conditions was estimated using a curve fitter online tool (http://statpages.info/nonlin.html), then the significance of the difference between the slopes of the KD and control conditions were estimated using an online statistic calculator (44).

For directional migration, the experiment was performed twice. Cells of CTRL and KD1 conditions were seeded on approximately 10 lanes of fibronectin matrix (200-μm width) per experiment. Cell trajectories were manually obtained using the "manual tracking" plugin of Fiji software and monitoring the displacement of the nucleus in each frame. We estimated θ, the absolute value in degrees of the angle generated by the displacement of the nucleus between two time points A and B as the absolute value of $\mathrm{Arctan}((y_B - y_A)/(x_B - x_A))$. Then directionality was calculated as the ratio between the sum of the absolute values of the angles θ and the distance traveled by the cell ($x_{MAX} - x_{MIN}$). The smaller this directionality value is the more persistent is the movement of the cell. As the directionality value increases, because of the increase of the sum of the angles generated by the cell, the more random its migration is. Three to four cells of the leading edge were tracked per fibronectin matrix. 56 cells were tracked in the first experiment ($n_{control} = 27$, $n_{KD} = 29$, $p = 0.02307$) and 71 in the second one ($n_{control} = 37$, $n_{KD} = 34$, $p = 0.00027$). A Student's t test was used to assess significant differences between the two conditions. Data were plotted using R.

RESULTS

Comparison of MS and RNA-seq Data from AKT1-depleted Cells Suggests the Existence of Pervasive Posttranslational Events Affecting the Deregulated Proteins/Genes—To obtain an overview of the molecular events dependent on AKT1 in pGCs, we silenced *Akt1* using RNA interference. RT-qPCR, and Western blotting analyses confirmed a depletion greater than 90% at the transcript level and of about 50% at the protein level in the KD conditions. MS analyses revealed 678 differentially expressed proteins ($p < 0.05$) between cells treated with the siRNAs targeting *Akt1* (four combinations of three different anti-*Akt1* siRNAs in duplicate, $n = 8$) and those treated with the scramble siRNA (three replicates) (Fig. 1, Supplemental Table S1; see Supplemental Table S2 for all protein and peptide identifications and Supplemental Table S3 for all

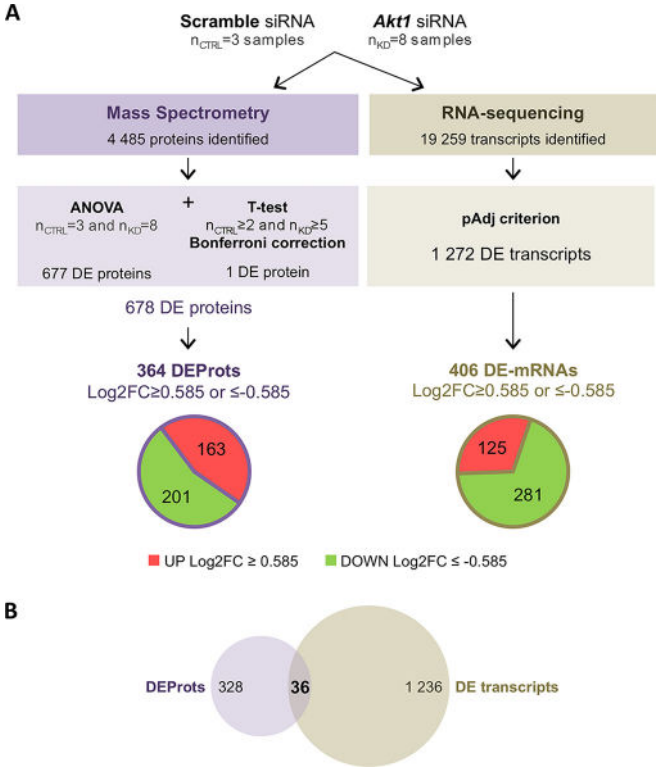

FIG. 1. **Comparison of mass spectrometry and RNA-sequencing data performed in murine primary granulosa cells.** (*A*) Three samples of pGCs transfected with scramble siRNA and eight samples (four combinations of three siRNA in duplicate) of pGCs depleted for *Akt1* were subjected to mass spectrometry and RNA-sequencing. Out of 4 485 proteins that were identified by MS, 678 proteins were considered to be differentially expressed, of which 364 had a Log2FC of variation equal or greater than 0.585 in both directions (DEProts). The downregulated subset comprised 163 proteins with a mean Log2FC = −0.92, whereas the 201 up-regulated proteins had mean Log2FC = 1.05. Out of 19,259 transcripts were identified by RNA-sequencing, 1,272 transcripts were considered differentially expressed between the KD and control conditions ($p < 0.05$), of which 406 had a Log2FC of variation equal or greater than 0.585 in both directions (DE-mRNAs, 281 were downregulated, with a mean Log2FC = −0.71, and 125 up-regulated with a mean Log2FC = 0.73). (*B*) Venn diagram representing the overlap between the deregulated proteins and the genes deregulated at the transcript level after *Akt1* depletion.

protein and peptide quantification). In our subsequent analyses, we focused on the 364 proteins having a Log2FC ≥ 0.585 or ≤ −0.585, which corresponds to a fold change ≥ 1.5 in either direction (DEProts). Specifically this subset included 163 downregulated and 201 up-regulated proteins (Fig. 1*A*, Supplemental Fig. S1). In parallel, the analysis of RNA-seq data revealed 1,272 differentially expressed transcripts (DE-mRNAs, $p < 0.05$) between KD and control cells (Fig. 1*A*, Supplemental Table S4). Among them, we focused on the 406 having a Log2FC ≥ 0.585 or ≤ −0.585, out of which 281 were downregulated and 125 up-regulated.

Among the 364 DEProts, 355 had a transcript identified in the RNA-seq data and only 36 corresponding transcripts were significantly deregulated (Fig. 1*B*). As further discussed below, this suggests the existence of pervasive posttranslational processes affecting the deregulated proteins. The expression of 25 proteins changed in the same direction as that of the corresponding transcript, and 11 changed in the opposite direction. The 25 proteins mentioned above involve regulators of cell cycle, gene expression, protein production, metabolism, intracellular transport, and the actin cytoskeleton (Supplemental Table S5).

Differentially phosphorylated peptides and kinases potentially acting downstream of AKT1—MS data revealed peptides with different posttranslational modifications and, as expected, phosphorylation. Thus, we aimed to identify the proteins differentially phosphorylated (DPhospho) after *Akt1* KD. The MS experiment allowed us to identify 250 phosphorylated peptides, but only 20 peptides appeared to be differentially phosphorylated between the KD and the control conditions (Supplemental Table S6; see Supplemental Table S2 for all protein and peptide identifications and Supplemental Table S3 for all protein and peptide quantification). To determine which of these peptides were actually differentially phosphorylated (*i.e.* not following a similar difference in protein expression), we compared their Log2FC phosphorylation with the Log2FC expression of the relevant proteins (Fig. 2*A*). We found that some of the peptides were perfectly aligned with the trend line of Fig. 2*A* (where differential phosphorylation correlates with differential expression) while others were not. To objectively identify the peptides for which changes in phosphorylation were independent of expression changes, we normalized the difference between Log2FC phosphorylation and Log2FC expression for each peptide and spotted the outliers (*i.e.* DPhospho peptides) as described in the "Materials and Methods" section. This allowed us to pinpoint 8 differentially phosphorylated peptides (DPhospho, $p < 0.05$) derived from β-catenin, RTN4, EEF1D, CALM1, GOT2, EIF2S2, SRRM2, and PTMA (Fig. 2*A*, Supplemental Table S6). According to GeneCards (45), such proteins are involved in the regulation of the cytoskeleton and cell adhesion, mRNA/protein production via splicing and translation processes, amino acid metabolism, immune function, and G-protein signaling. The peptides derived from β-catenin, RTN4, EEF1D, and CALM1 showed a decreased phosphorylation level upon *Akt1* KD. These proteins can thus be potential direct targets of AKT1. In contrast, those derived from GOT2, EIF2S2, SRRM2, and PTMA displayed an increased phosphorylation after *Akt1* silencing. Such proteins are thus potential targets either of kinases inhibited by AKT1 or of phosphatases activated by AKT1.

Next, we used GPS3.0 and PhosphoNET prediction tools to uncover candidate kinases that could be responsible for the phosphorylation of the DPhospho peptides. We kept the kinases predicted by both softwares to regulate at least three DPhospho peptides and that were expressed in the pGCs according to our MS experiment ($n = 12$ kinases, AKT1 being one of them). We also included in our analysis the kinases and

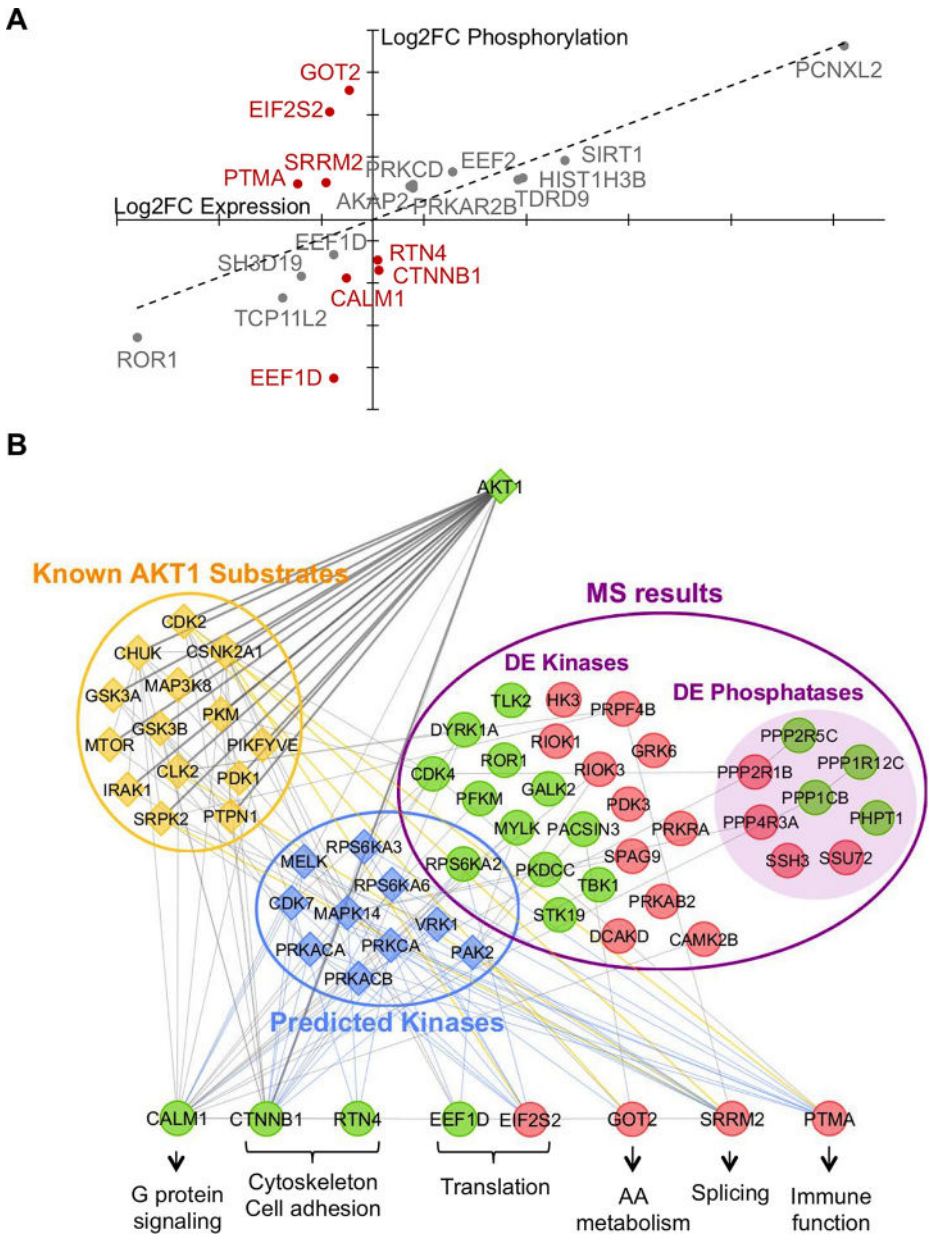

FIG. 2. **Identification of the peptides differentially phosphorylated after *Akt1* depletion.** (*A*) The scatterplot of the Log2FC values resulting from differentially expressed proteins and differentially phosphorylated peptides reveals two distinct populations of phosphorylated peptides. In gray, the peptides displaying the same variation of phosphorylation and expression were not considered to be differentially phosphorylated. In deep red, the peptides displaying a variation of phosphorylation independent of the variation of the expression of the relevant proteins were considered as DPhospho peptides. (*B*) Model for the regulation of the DPhospho peptides. The network was built using GeneMania and Cytoscape searching for the PPI existing between the 8 DPhospho peptides, the 12 predicted kinases, the 30 DE kinases and DE phosphatases, and the kinases referenced in the PhosphoSite Plus database as AKT1 substrates (known AKT1 substrates, $n = 46$). Only the nodes connected to the DPhospho peptides were taken into account. GeneCards helped with the attribution of the DPhospho peptides to cellular processes. Green nodes: down-regulated/phosphorylated. Red: up-regulated/phosphorylated. Bold edges show AKT1 direct targets. Blue edges are predicted by GPS3.0 and PhosphoNET. Light orange edges connect up-regulated DPhospho peptides with known kinase substrates of AKT1.

phosphatases differentially expressed in the MS data (DE kinases and phosphatases). Next, we used GeneMania to build a network based on the protein-protein interactions (PPI) occurring between the 8 DPhospho peptides, the 12 predicted kinases, 30 DE kinases and phosphatases, and those referenced in the PhosphoSite Plus database as being AKT1 substrates ($n = 46$). As a result, we obtained a highly connected PPI network involving a series of kinases and phosphatases that could mediate AKT1 (direct and indirect) action on the DPhospho peptides (Fig. 2*B*).

Pathways dependent on AKT1 in mouse granulosa cells—To get a global picture of the cellular pathways responding to AKT1 in mouse pGCs, we employed GeneMania to investigate the connections existing between the DEProts and DPhospho peptides. Enrichment analyses were performed using the Gene Set Enrichment Analysis database (46, 47). In addition, we used GeneCards to explore the biological functions of deregulated proteins not involved in the enriched processes. As expected, numerous pathways were significantly affected by *Akt1* depletion (Fig. 3, Supplemental Table S7). These pathways are related to gene expression and protein production [translation (p = 2.86E-3), ribosome biogenesis (p = 5.22E-3), rRNA processing (p = 4.25E-4), mitochondrial translation (p = 2.02E-2), mRNA surveillance (p = 3.48E-2), RNA splicing (p = 1.62E-2)], metabolism [of lipids and lipoproteins (p = 2.78E-5), glucose (p = 5.32E-4) and of amino acid and derivatives (p = 1.04E-2)], and intracellular transport [(vesicle-mediated transport (p = 7.2E-3) and mitochondrial protein import (p = 5.93E-3)]. We also found significant enrichment of the pathways related to respiratory electron transport (p = 4.07E-2), posttranslational modifications (PTM, p = 2.16E-3), apoptosis (p = 6.24E-4), cell cycle (p = 1.61E-2), actin cytoskeleton regulation (p = 1.47E-2), and focal adhesion (p = 1.06E-2).

In silico analyses of the DE-mRNAs point to transcription factors potentially targeted by AKT1—The transcriptional impact of AKT1 can be due to an indirect modulation of the expression of a set of TFs and/or their posttranslational modification. In the former category, we found 28 TFs and regulators whose expression was deregulated by the AKT1 depletion. Such DE-TFs belonged to different categories: specific TFs (CREB1, CEBPB, FOXP1, NFκB2, PELP1, TFAM, and ZBED6), general TFs (GTF2E2), epigenetic effectors (BRD8, CBX1, ENY2, HMGB2, MECP2, and PHF6), and transcription co-factors/regulators (ASCC1, CTBP1, DDX1, DHX36, DDX3X, DDX54, ELP4, HNRNPK, MED23, MED4, PIR, RBPMS, SFR1, and TLE4).

To identify other TFs whose direct and indirect targets in other tissues were also differentially expressed according to our RNA-seq data, we submitted the list of the 406 DE-mRNAs to the EnrichR database. This analysis allowed us to uncover nine TFs, namely, GATA4, RNF2, NFE2L2, CREB1, TFAP2C, HSF1, WT1, TCOF1, and EMX2, which become direct or indirect candidate targets of AKT1 themselves (Fig. 4*A*, Supplemental Table S8). Interestingly, CREB1 is a known target of AKT1 that appears downregulated in our MS data. We further studied the involvement of such TFs as potential effectors acting downstream of AKT1 by assessing whether some of their known targets (according to EnrichR, that are also deregulated in our RNA-seq data) were indeed deregulated after their own KD in mouse granulosa cells. To conduct this study, we focused on DE-mRNAs known to be expressed at more than five reads per kilobase per million mapped reads in the mouse ovary (according to the Encyclopedia of DNA Elements (ENCODE) consortium transcriptome data). RNA-seq data for the selected target genes were validated by RT-qPCR in mouse pGCs KD for *Akt1*. For simplicity, we performed a similar experiment in AT29C cells that are widely used as a model of granulosa cell biology (37). Moreover, the proteomes of both cell types are quite similar (Pearson's r = 0.70 and two-tailed $p < 0.001$) (Supplemental Fig. S2). As expected, we obtained a strong correlation (Pearson's r = 0.75, two-tailed $p < 0.001$) between the *AKT1* KD results for a set of 35 genes (targets in other tissues of the TFs mentioned above) in the two cell types (Fig. 4*B*). Thus, we performed the KD of several TFs of interest, *Creb1*, *Nfkb2*, and *Wt1*, in the AT29C cells (Fig. 4*C*, Supplemental Fig. S3). The KD of *Creb1* produced a similar deregulation of *Ecm1*, *Pdlim7*, *Ppib*, and *S100a16* as the depletion of *Akt1* (Fig. 4*D*). Thus, it is likely that AKT1 regulates these genes through its action on CREB1 expression. As *Crip1*, *Smarca2*, and *Ups11* did not change in the same direction between *Creb1* KD and *Akt1* KD, it is unlikely that AKT1 regulates these genes through its action on CREB1 in these cell lines. We conducted similar KD experiments on *Nfkb2,* which is a known target of AKT1 and whose expression is up-regulated according to the MS data and on *Wt1,* which is a key factor of granulosa cell lineage differentiation and ovarian function (48). The latter displayed the biggest absolute overlap between the DE-mRNAs and WT1 direct and indirect targets according to EnrichR database. As NFκB2 was up-regulated following *Akt1* silencing, we expected that the effect of its KD on its targets would mirror the results of *Akt1* depletion. Consistently, the up-regulation of *Cdhr1* and *Ovgp1* observed after *Akt1* KD could be the consequence of its regulation of NFκB2. The KD of *Wt1* had a similar effect on *Capn1*, *Eri3*, *Mvd*, *Ppib*, and *Tmem109* as the *Akt1* depletion (Fig. 4*D*). Thus, we hypothesize that AKT1 regulates these genes via a direct or indirect action on WT1.

Granulosa cells depleted for Akt1 show altered migration patterns—As several DEProts were related to cell adhesion, cytoskeleton regulation and extracellular matrix organization (Fig. 3, Supplemental Table S5), which are critical processes for cell migration, we studied the migration potential of AT29C cells depleted for *Akt1*. The velocity of migration was assessed using a scratch-wound assay (Fig. 5*A*). Specifically, the speed of wound healing was followed by measuring the slope of the line representing the area noncovered by migrating cells (relative to the initial wounded surface) *versus* time in both conditions (control and KD). Interestingly, the slope was significantly steeper in the KD (slope = -0.078 h^{-1}) compared with the control condition (slope = -0.064 h^{-1}) (*t* test, p = 5.5E-4) meaning that *Akt1* depletion increases migration velocity in this experimental setting. We also studied directional migration on a fibronectin matrix by using an insert-

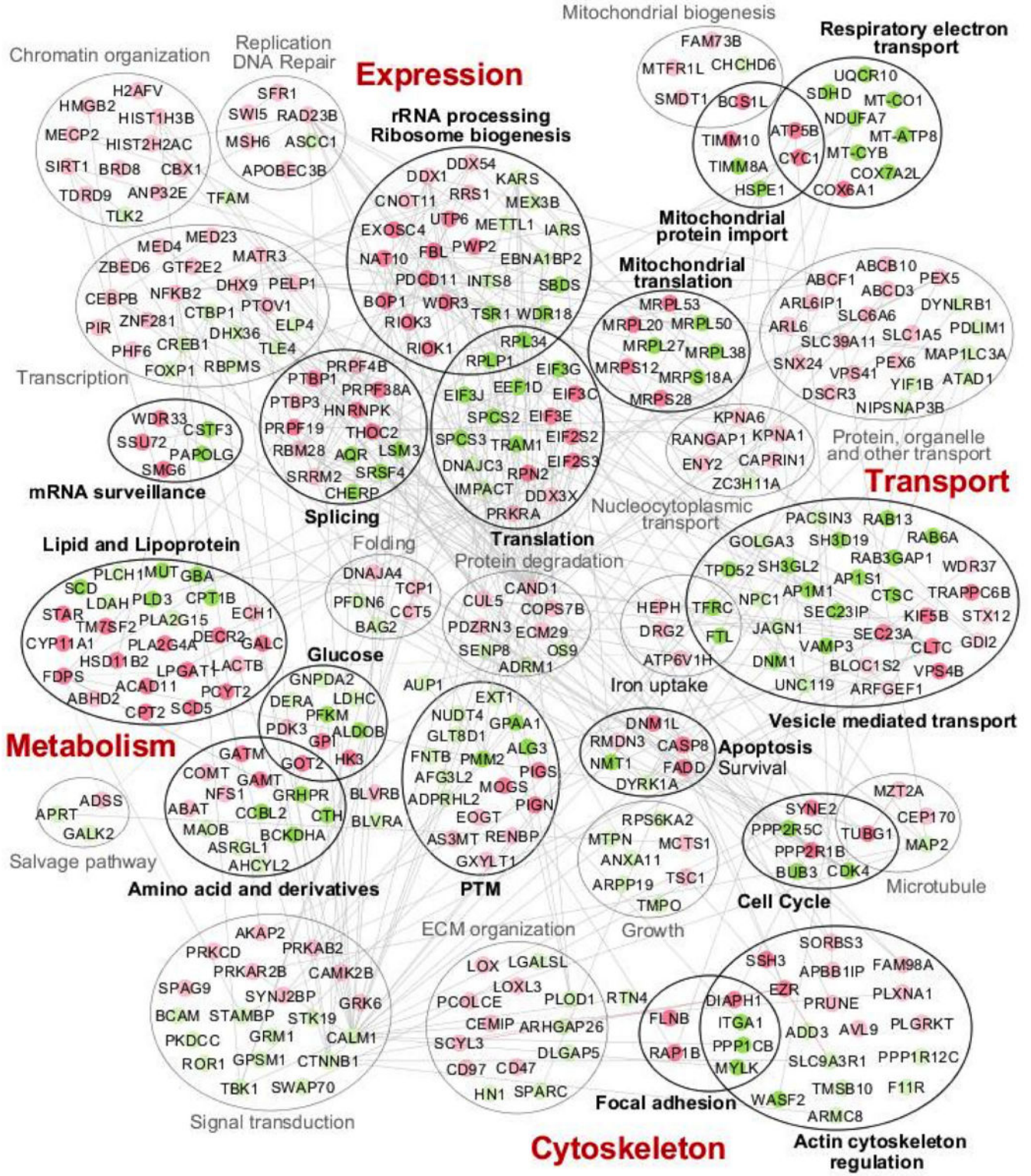

FIG. 3. **Pathways responding to *Akt1* depletion.** The list of DEProts and DPhospho peptides obtained after *Akt1* depletion was submitted to GeneMania and GSEA to gain insights into the pathways affected by this perturbation. Circles filled with dark green/red color represent downregulated/up-regulated proteins involved in significantly enriched pathways/processes (surrounded by black ellipses with bold labels). The light green/red circles represent proteins that were manually assigned to different cellular processes following GeneCards (surrounded by gray ellipses). The main pathways impacted concern gene expression and protein production, metabolism, cytoskeleton regulation, and transport.

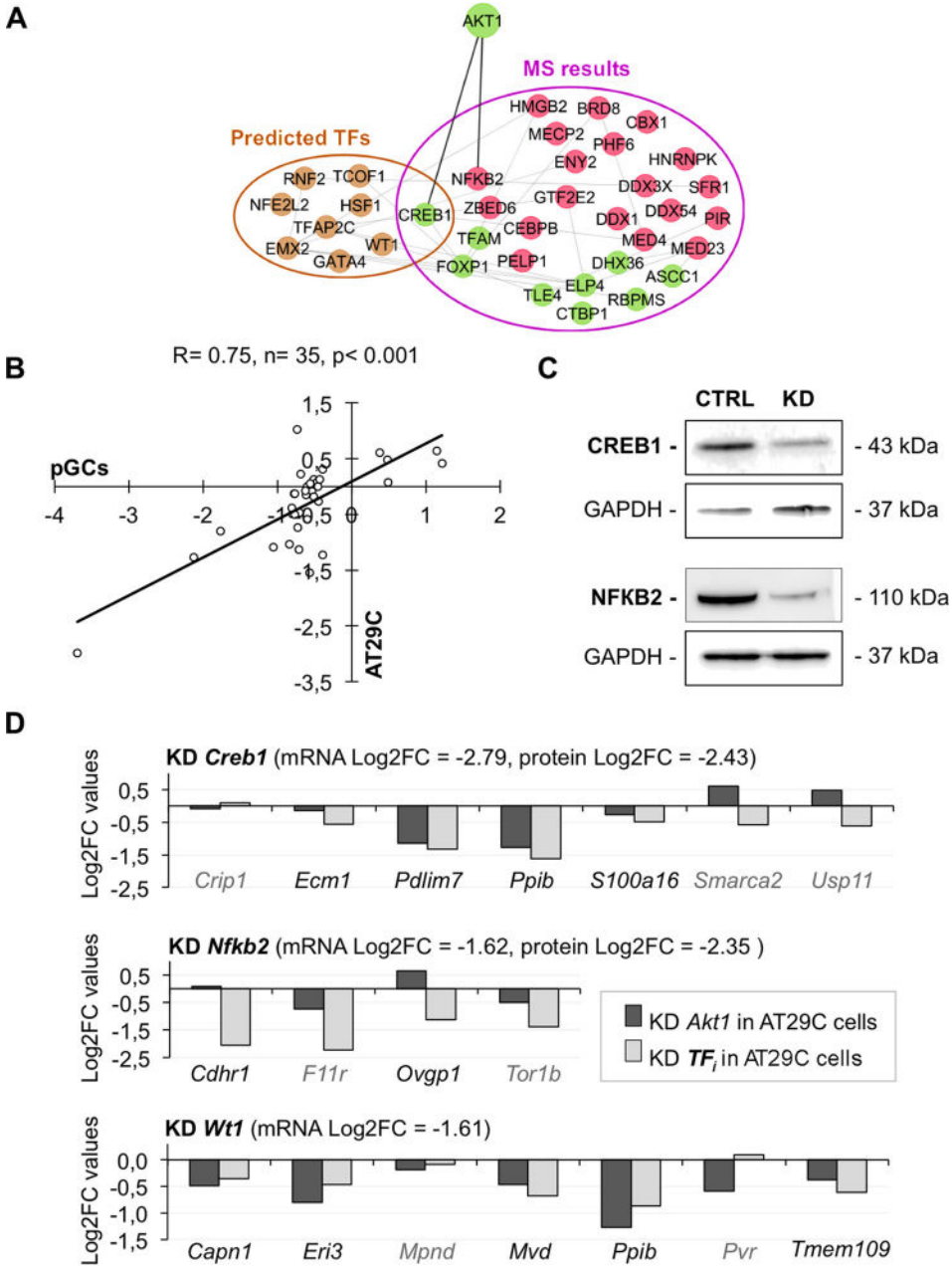

FIG. 4. **Exploration of the genomic effects of AKT1.** (*A*) Model for the regulation of the DE-mRNAs. The DE-mRNAs could result from deregulation of TFs and regulators identified by MS (MS results) or predicted by EnrichR (predicted TFs). (*B*) Scatterplot of the Log2FC values for the 35 differentially expressed genes in primary granulosa cells or in AT29C after *Akt1* depletion, corresponding to the potential transcriptional targets of *Creb1*, *Nfkb2*, and *Wt1* identified *in silico* using EnrichR. A significant correlation between the two cell types ($r = 0.75$, $p < 0.001$) is apparent. (*C*) Efficiency of CREB1 and NFκB2 depletion after 30 h of KD. The mean KD efficiency studied by Western blotting is of about 80% for each TF. (*D*) Effect of *Creb1*, *Nfkb2*, or *Wt1* down-regulation on the expression of transcripts dependent on *Akt1*. The KD of *Creb1*, *Nfkb2*, or *Wt1* was performed in AT29C cells. In each KD condition, we assessed the expression of the DE-mRNAs predicted by EnrichR to be the target of the TF of interest. Dark gray bars: Log2FC values obtained by RT-qPCR after *Akt1* depletion in AT29C cells. Light gray bars: Log2FC values obtained by RT-qPCR after depletion of the TF of interest (TF_i) in AT29C cells.

removal approach (Figs. 5*B*–5*D*). Specifically, 24 h after insert removal, we studied the ability of KD and control cells at the leading edge to migrate by tracking them. We assessed the persistent *versus* random behavior of migration by calculating the sum of the absolute values of the angles θ generated by the movements of the nuclei at various time points divided by the distance *d* traveled by the relevant nuclei (Fig. 5*B*). AT29C cells KD for *Akt1* showed more random motility when compared with the control condition (*t* test, $p = 0.023$, Figs. 5*C* and 5*D*).

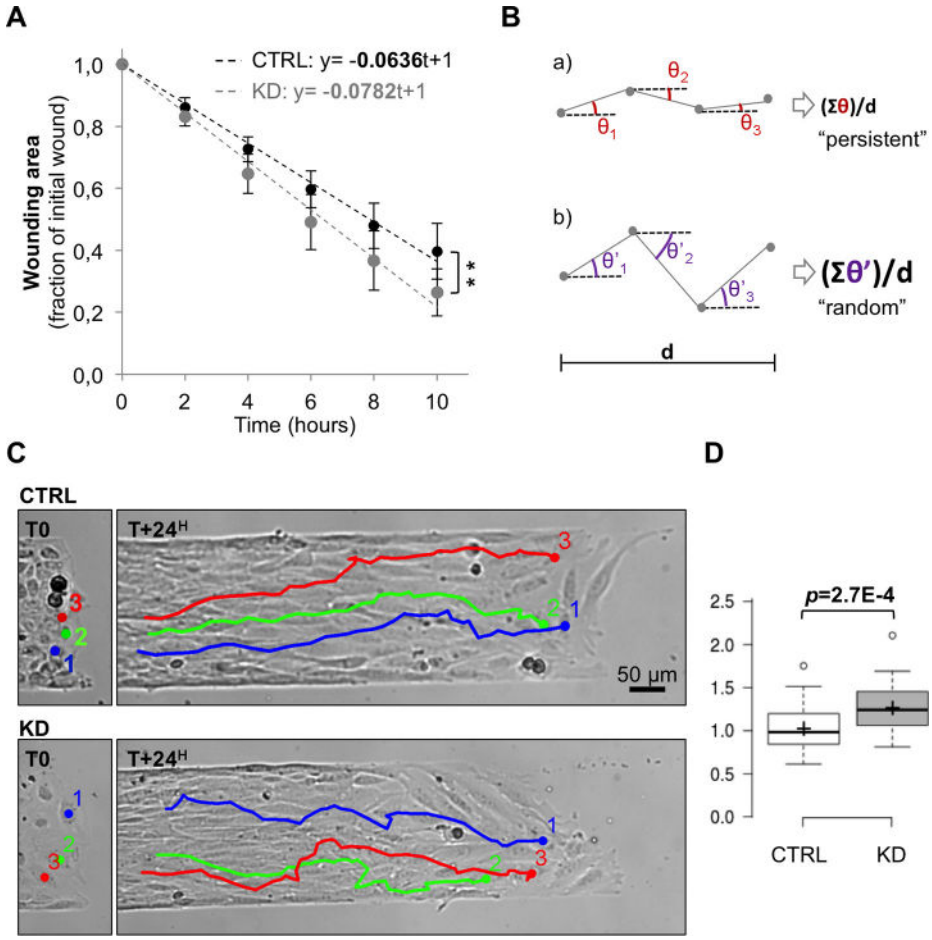

FIG. 5. ***Akt1* depletion alters the migration patterns of AT29C cells.** (*A*) Result of the scratch-wound assay. We plotted the mean wounded cell-free area expressed as a fraction of that of the initial wound, in control and KD conditions. The experiment was repeated three times. The slopes of the lines (representing the rate of decrease of the wounded/cell free area) were significantly different (p = 5.5E-4). (*B*) Outline of our analysis of directional persistence migration. The persistent *versus* random behavior of migration was determined by calculating the sum of the absolute value in degrees of the angles θ, generated by the movements of the nucleus between two time points A and B divided by the distance traveled by the cell (x_{MAX}-x_{MIN}). In the case (a), the angles θ generated by the cell migration are smaller than in the case (b). Thus, the smaller is the value obtained, the more persistent is the trajectory. (*C*) Example of AT29C cell trajectories on fibronectin patterns after *Akt1* depletion or not. The directionality of AT29C cell migration was measured after tracking the displacement of each nucleus. (*D*) Quantification of the directionality of AT29C cell migration after *Akt1* depletion. Increased random migration is observed in the KD condition compared with the control. The experiment was performed twice, 56 cells were tracked in the first experiment ($n_{control}$ = 27, n_{KD} = 29, p = 0.02307) and 71 in the second one ($n_{control}$ = 37, n_{KD} = 34, p = 0.00027). A Student's t test was used to assess significant differences between the two conditions.

DISCUSSION

Here, we used RNAi to deplete *Akt1* in mouse pGCs, then performed RNA-seq and MS experiments to obtain an overview of the cellular pathways and molecular events depending on this kinase in this ovarian cell type that supports germ cell development. We found that the majority of DEProts were not deregulated at the transcript level, suggesting the existence of a posttranscriptional events impacting on the translation or the stability of such proteins. Consistently, among the main pathways responding to AKT1 depletion, we found significant enrichment of protein production processes, comprising mRNA surveillance and translation (Supplemental Table S7, Fig. 3). Proteins involved in the regulation of protein folding and degradation were also significantly deregulated.

We found several TFs and regulators affected by *Akt1* depletion that could explain the transcriptional changes observed in the RNA-seq data. In addition, they could be due, at least in part, to posttranslational modifications of TFs not identified in MS data. In the latter category, we identified nine TFs through *in silico* analyses as they share transcriptional targets with AKT1 when depleted in other models (Supplemental Table S8). It is noteworthy that several of them have been shown to play key roles in ovarian development and function (such as EMX2 (49), GATA4 (50), WT1 (48), RNF2 (51)) or in the stress response in the ovary (NFE2L2 (52), HSF1 (53)). We confirmed that the KD of *Creb1* or *Wt1* in AT29c cells produced similar effects for a subset of transcriptional targets as those of *Akt1*. Thus, we speculate that CREB1 and WT1 act

downstream of AKT1 to mediate some of its genomic effects also in primary granulosa cells. Interestingly, activating phosphorylation of CREB1 by AKT has been reported in human embryonic kidney 293T cells and leads to the regulation of the expression of genes involved in cell survival (13). Besides, AKT1 has been shown to increase WT1 expression in breast cancer cells to regulate cell cycle progression and apoptosis (54).

Our MS experiment was not designed to focus on DPhospho peptides (*i.e.* through artificial enrichment) but to provide an overview of the global deregulation occurring at the protein level. However, we were able to detect eight DPhospho peptides (Supplemental Table S6). As noted above, those derived from β-catenin, RTN4, EEF1D, and CALM1 could represent potential direct targets of AKT1. Consistently, β-catenin, a key downstream effector of the WNT signaling pathway, is a known substrate of AKT1. Indeed, phosphorylation of β-catenin by AKT1 at Ser552 increases its transcriptional activity (55). According to PhosphoNET, Ser675 is also predicted to be phosphorylated by AKT1. Along similar lines, Ser15 of RTN4 (reticulon 4), a protein involved in membrane trafficking, has been shown to be sensitive to mTORC1 inhibition (56). As mTORC1 is regulated by AKT1, RTN4 phosphorylation could at least indirectly depend on AKT1 via mTORC1. Regarding the two other downregulated DPhospho peptides, EEF1D and CALM1, we are the first to report their sensitivity to AKT1 (depletion), and further work is required to explore the biological relevance of our findings. The peptides derived from GOT2, EIF2S2, SRRM2, and PTMA are expected to be indirect targets of AKT1. These DPhospho peptides can be substrates of kinases/phosphatases deregulated upon *Akt1* depletion or of kinases/phosphatases that we could have missed in our MS data (Fig. 2). Notably, three of the four up-regulated DPhospho peptides, namely EIF2S2, SRRM2, and PTMA, make PPI with known kinases substrates of AKT1 that we did not identify in our MS experiment (Fig. 2, light orange edges). We thus make the testable hypothesis that their differential phosphorylation can be due to the action of these kinases.

Not surprisingly, multiple biological processes were impacted by *Akt1* depletion. We found significant enrichment signals for processes related to gene expression and protein production, metabolism, transport, and cell growth (Fig. 3). Regarding cell growth, by inhibiting phosphorylation of TSC2, AKT1 ensures mTORC1 activation (57, 58), which induces activation of S6K1/2 and inhibition of 4E-BP1 to stimulate both ribosome biogenesis and translation initiation (59). Interestingly, we found an up-regulation of TSC1 at the protein level but not at the transcript level, suggesting that *Akt1* depletion leads to increased translation/stability of the protein. It is known that TSC1 forms a heterodimeric complex with TSC2 (60), which is negatively regulated by 14–3-3beta after AKT1 phosphorylation (61) and finally degraded by the proteasome (62). We speculate that the increased TSC1 expression observed after *Akt1* depletion could mimic an increased availability of TSC2 even if the protein was not detected in the MS experiment. More generally, the DEProts related to ribosome biogenesis, translation, and growth constitute novel candidate targets of the AKT1/TSC1,2/mTORC1/S6K1,2/4E-BP1 pathway. In sum, our proteomic approach in pGCs confirms the well-documented implication of AKT1 in the regulation of metabolism, cell cycle, survival/apoptosis (reviewed in (1)), actin cytoskeleton (22, 23) and DNA repair (63), and provides new links to be explored, namely, between AKT1 and intracellular transport or mitochondrial physiology.

On cell biology grounds, we found that the migration behavior of AT29C cells depleted for *Akt1* was different from that of control cells (Fig. 5). We noticed that *Akt1* depletion leads to a faster healing in scratch-wound assays, which is in line with several studies that have pinpointed the implication of Akt signaling in the regulation of processes controlling migration, actin cytoskeleton organization, cell-to-cell adhesion, or extracellular matrix remodeling. Indeed, several studies have documented an antimigration role for AKT1. One of them, performed in the human epithelial breast cancer cell line MCF-10, revealed that silencing of *Akt1* enhanced their migration (64). Similarly, the overexpression of activated AKT1 in another breast cancer cell line provoked reduced motility and invasion (65). However, AKT1 seems to have opposite effects depending on the cell type studied and/or whether the kinase is overexpressed in a constitutively active form or silenced (reviewed in (24, 66)). For instance, constitutively active AKT1 was shown to promote migration by activation of Girdin in kidney epithelial cells (22). The impact of AKT1 on migration may depend on the cell type and on the experimental conditions. For instance, in our insert removal experiment, we failed to detect any significant difference in the mean migration velocity between KD and control cells. However, in the very same experiment AT29C cells depleted for *Akt1* did show altered directional migration (Fig. 5). Indeed, by manually tracking individual cell migration, we found that *AKT1*-KD AT29C cells at the leading edge displayed a more random motility than the one of the control cells. Directional migration depends on the ability of the cell to polarize and reshape its cytoskeleton and its adhesion in response to intrinsic or extrinsic (environmental) regulation (67). In our MS data, some of the DEProts involved in focal adhesion and cytoskeleton regulation could explain the observed phenotype. Moreover, the PI3K/AKT pathway is known to positively regulate cell polarity (68, 69), and *Akt1* deficiency has been shown to reduce migration directionality in breast cancer cells (70). Our results thus confirm and extend previous observations.

In conclusion, this study maps the molecular effects of *Akt1* depletion at the protein and transcript levels in mouse granulosa cells. It confirms and extends the role of this kinase in critical cellular processes such directional migration. Our experimental and *in silico* analyses provide a series of new substrate candidates that deserve further investigation.

Acknowledgments—We thanks Dr A. Glentis for kind help with migration assays and Dr S. Caburet for her help with Cytoscape. We thank the CNRS' IMAGIF platform for the RNA-seq implementation.

DATA AVAILABILITY

The MS proteomics data have been deposited to the ProteomeXchange Consortium via the PRIDE (43) partner repository with the dataset identifier PXD012548 as .raw files, Proteome Discoverer 2.1 .pdResult file, associated pep.xml and xlsx files, label-free report generated by Progenesis QI. For RNA-sequencing results, data are available at Gene Expression Omnibus, accession number GSE130187.

* This work was supported by the University Paris-Diderot, by the Centre National de la Recherche Scientifique, by GEFLUC and from the Fondation pour la Recherche Médicale grant: [DEQ20150331757].

[S] This article contains supplemental material Tables S1–S8 and Figs. S1–S3.

¶ To whom correspondence may be addressed: Institut Jacques Monod. 15 rue Hélène Brion, 75013 Paris, France. Tel.: 33 6 03 51 67 46; E-mail: reiner.veitia@ijm.fr.

‖ To whom correspondence may be addressed: Institut Jacques Monod. 15 rue Hélène Brion, 75013 Paris, France. Tel.: 33 6 03 51 67 46; E-mail: anne-laure.todeschini@ijm.fr.

Author contributions: M.E., A.-L.T., and R.A.V. designed research; M.E., L.H., and B.L. performed research; M.E., L.H., B.L., T.L., and R.A.V. analyzed data; and M.E., A.-L.T., and R.A.V. wrote the paper.

REFERENCES

1. Manning, B. D., and Cantley, L. C. (2007) AKT/PKB signaling: Navigating downstream. *Cell* **129,** 1261–1274
2. Cecconi, S., Mauro, A., Cellini, V., and Patacchiola, F. (2012) The role of Akt signalling in the mammalian ovary. *Int. J. Dev. Biol.* **56,** 809–817
3. Dummler, B., and Hemmings, B. A. (2007) Physiological roles of PKB/Akt isoforms in development and disease. *Biochem. Soc. Trans.* **35,** 231–235
4. Gonzalez, E., and McGraw, T. E. (2009) The Akt kinases: Isoform specificity in metabolism and cancer. *Cell Cycle* **8,** 2502–2508
5. Alessi, D. R., Deak, M., Casamayor, A., Caudwell, F. B., Morrice, N., Norman, D. G., Gaffney, P., Reese, C. B., MacDougall, C. N., Harbison, D., Ashworth, A., and Bownes, M. (1997) 3-Phosphoinositide-dependent protein kinase-1 (PDK1): Structural and functional homology with the Drosophila DSTPK61 kinase. *Curr. Biol.* **7,** 776–789
6. Sarbassov, D. D., Guertin, D. A., Ali, S. M., and Sabatini, D. M. (2005) Phosphorylation and regulation of Akt/PKB by the rictor-mTOR complex. *Science* **307,** 1098–1101
7. Ersahin, T., Tuncbag, N., and Cetin-Atalay, R. (2015) The PI3K/AKT/mTOR interactive pathway. *Mol. Biosyst.* **11,** 1946–1954
8. Datta, S. R., Dudek, H., Tao, X., Masters, S., Fu, H., Gotoh, Y., and Greenberg, M. E. (1997) Akt phosphorylation of BAD couples survival signals to the cell-intrinsic death machinery. *Cell* **91,** 231–241
9. Mayo, L. D., and Donner, D. B. (2001) A phosphatidylinositol 3-kinase/Akt pathway promotes translocation of Mdm2 from the cytoplasm to the nucleus. *Proc. Natl. Acad. Sci. U.S.A.* **98,** 11598–11603
10. Sunters, A., Fernández de Mattos, S., Stahl, M., Brosens, J. J., Zoumpoulidou, G., Saunders, C. A., Coffer, P. J., Medema, R. H., Coombes, R. C., and Lam, E. W.-F. (2003) FoxO3a transcriptional regulation of Bim controls apoptosis in paclitaxel-treated breast cancer cell lines. *J. Biol. Chem.* **278,** 49795–49805
11. Gilley, J., Coffer, P. J., and Ham, J. (2003) FOXO transcription factors directly activate bim gene expression and promote apoptosis in sympathetic neurons. *J. Cell Biol.* **162,** 613–622
12. Brunet, A., Bonni, A., Zigmond, M. J., Lin, M. Z., Juo, P., Hu, L. S., Anderson, M. J., Arden, K. C., Blenis, J., and Greenberg, M. E. (1999) Akt promotes cell survival by phosphorylating and inhibiting a Forkhead transcription factor. *Cell* **96,** 857–868
13. Du, K., and Montminy, M. (1998) CREB is a regulatory target for the protein kinase Akt/PKB. *J. Biol. Chem.* **273,** 32377–32379
14. Kane, L. P., Shapiro, V. S., Stokoe, D., and Weiss, A. (1999) Induction of NF-kappaB by the Akt/PKB kinase. *Curr. Biol.* **9,** 601–604
15. Shin, I., Yakes, F. M., Rojo, F., Shin, N.-Y., Bakin, A. V., Baselga, J., and Arteaga, C. L. (2002) PKB/Akt mediates cell-cycle progression by phosphorylation of p27(Kip1) at threonine 157 and modulation of its cellular localization. *Nat. Med.* **8,** 1145–1152
16. Diehl, J. A., Cheng, M., Roussel, M. F., and Sherr, C. J. (1998) Glycogen synthase kinase-3beta regulates cyclin D1 proteolysis and subcellular localization. *Genes Dev.* **12,** 3499–3511
17. Dibble, C. C., and Cantley, L. C. (2015) Regulation of mTORC1 by PI3K signaling. *Trends Cell Biol.* **25,** 545–555
18. Cong, L. N., Chen, H., Li, Y., Zhou, L., McGibbon, M. A., Taylor, S. I., and Quon, M. J. (1997) Physiological role of Akt in insulin-stimulated translocation of GLUT4 in transfected rat adipose cells. *Mol. Endocrinol.* **11,** 1881–1890
19. Wang, Q., Somwar, R., Bilan, P. J., Liu, Z., Jin, J., Woodgett, J. R., and Klip, A. (1999) Protein kinase B/Akt participates in GLUT4 translocation by insulin in L6 myoblasts. *Mol. Cell. Biol.* **19,** 4008–4018
20. Beurel, E., Grieco, S. F., and Jope, R. S. (2015) Glycogen synthase kinase-3 (GSK3): Regulation, actions, and diseases. *Pharmacol. Ther.* **148,** 114–131
21. Dimmeler, S., Fleming, I., Fisslthaler, B., Hermann, C., Busse, R., and Zeiher, A. M. (1999) Activation of nitric oxide synthase in endothelial cells by Akt-dependent phosphorylation. *Nature* **399,** 601–605
22. Enomoto, A., Murakami, H., Asai, N., Morone, N., Watanabe, T., Kawai, K., Murakumo, Y., Usukura, J., Kaibuchi, K., and Takahashi, M. (2005) Akt/PKB regulates actin organization and cell motility via Girdin/APE. *Dev. Cell* **9,** 389–402
23. Vandermoere, F., El Yazidi-Belkoura, I., Demont, Y., Slomianny, C., Antol, J., Lemoine, J., and Hondermarck, H. (2007) Proteomics exploration reveals that actin is a signaling target of the kinase Akt. *Mol. Cell. Proteomics* **6,** 114–124
24. Xue, G., and Hemmings, B. A. (2013) PKB/Akt-dependent regulation of cell motility. *J. Natl. Cancer Inst.* **105,** 393–404
25. Kim, D., Kim, S., Koh, H., Yoon, S. O., Chung, A. S., Cho, K. S., and Chung, J. (2001) Akt/PKB promotes cancer cell invasion via increased motility and metalloproteinase production. *FASEB J.* **15,** 1953–1962
26. Altomare, D. A., and Testa, J. R. (2005) Perturbations of the AKT signaling pathway in human cancer. *Oncogene* **24,** 7455–7464
27. Samuels, Y., Wang, Z., Bardelli, A., Silliman, N., Ptak, J., Szabo, S., Yan, H., Gazdar, A., Powell, S. M., Riggins, G. J., Willson, J. K. V., Markowitz, S., Kinzler, K. W., Vogelstein, B., and Velculescu, V. E. (2004) High frequency of mutations of the PIK3CA gene in human cancers. *Science* **304,** 554
28. Hyun, T., Yam, A., Pece, S., Xie, X., Zhang, J., Miki, T., Gutkind, J. S., and Li, W. (2000) Loss of PTEN expression leading to high Akt activation in human multiple myelomas. *Blood* **96,** 3560–3568
29. Stemke-Hale, K., Gonzalez-Angulo, A. M., Lluch, A., Neve, R. M., Kuo, W.-L., Davies, M., Carey, M., Hu, Z., Guan, Y., Sahin, A., Symmans, W. F., Pusztai, L., Nolden, L. K., Horlings, H., Berns, K., Hung, M.-C., van de Vijver, M. J., Valero, V., Gray, J. W., Bernards, R., Mills, G. B., and Hennessy, B. T. (2008) An integrative genomic and proteomic analysis of PIK3CA, PTEN, and AKT mutations in breast cancer. *Cancer Res.* **68,** 6084–6091
30. Kandoth, C., McLellan, M. D., Vandin, F., Ye, K., Niu, B., Lu, C., Xie, M., Zhang, Q., McMichael, J. F., Wyczalkowski, M. A., Leiserson, M. D. M., Miller, C. A., Welch, J. S., Walter, M. J., Wendl, M. C., Ley, T. J., Wilson, R. K., Raphael, B. J., and Ding, L. (2013) Mutational landscape and significance across 12 major cancer types. *Nature* **502,** 333–339
31. Carpten, J. D., Faber, A. L., Horn, C., Donoho, G. P., Briggs, S. L., Robbins, C. M., Hostetter, G., Boguslawski, S., Moses, T. Y., Savage, S., Uhlik, M., Lin, A., Du, J., Qian, Y.-W., Zeckner, D. J., Tucker-Kellogg, G., Touchman, J., Patel, K., Mousses, S., Bittner, M., Schevitz, R., Lai, M.-H. T., Blanchard, K. L., and Thomas, J. E. (2007) A transforming mutation in the pleckstrin homology domain of AKT1 in cancer. *Nature* **448,** 439–444
32. Bessière, L., Todeschini, A.-L., Auguste, A., Sarnacki, S., Flatters, D., Legois, B., Sultan, C., Kalfa, N., Galmiche, L., and Veitia, R. A. (2015) A hot-spot of in-frame duplications activates the oncoprotein AKT1 in juvenile granulosa cell tumors. *EBioMedicine* **2,** 421–431
33. Auguste, A., Bessière, L., Todeschini, A.-L., Caburet, S., Sarnacki, S., Prat, J., D'angelo, E., De La Grange, P., Ariste, O., Lemoine, F., Legois, B.,

Sultan, C., Zider, A., Galmiche, L., Kalfa, N., and Veitia, R. A. (2015) Molecular analyses of juvenile granulosa cell tumors bearing AKT1 mutations provide insights into tumor biology and therapeutic leads. *Hum. Mol. Genet.* **24,** 6687–6698
34. Brown, C., LaRocca, J., Pietruska, J., Ota, M., Anderson, L., Smith, S. D., Weston, P., Rasoulpour, T., and Hixon, M. L. (2010) Subfertility caused by altered follicular development and oocyte growth in female mice lacking PKB alpha/Akt1. *Biol. Reprod.* **82,** 246–256
35. Monniaux, D. (2016) Driving folliculogenesis by the oocyte-somatic cell dialog: Lessons from genetic models. *Theriogenology* **86,** 41–53
36. Georges, A., L'Hôte, D., Todeschini, A. L., Auguste, A., Legois, B., Zider, A., and Veitia, R. A. (2014) The transcription factor FOXL2 mobilizes estrogen signaling to maintain the identity of ovarian granulosa cells. *eLife* **4,** 3
37. Dutertre, M., Gouédard, L., Xavier, F., Long, W. Q., di Clemente, N., Picard, J. Y., and Rey, R. (2001) Ovarian granulosa cell tumors express a functional membrane receptor for anti-Müllerian hormone in transgenic mice. *Endocrinology* **142,** 4040–4046
38. Schindelin, J., Arganda-Carreras, I., Frise, E., Kaynig, V., Longair, M., Pietzsch, T., Preibisch, S., Rueden, C., Saalfeld, S., Schmid, B., Tinevez, J.-Y., White, D. J., Hartenstein, V., Eliceiri, K., Tomancak, P., and Cardona, A. (2012) Fiji: An open-source platform for biological-image analysis. *Nat. Methods* **9,** 676–682
39. Shannon, P., Markiel, A., Ozier, O., Baliga, N. S., Wang, J. T., Ramage, D., Amin, N., Schwikowski, B., and Ideker, T. (2003) Cytoscape: A software environment for integrated models of biomolecular interaction networks. *Genome Res.* **13,** 2498–2504
40. Gavard, J., Lambert, M., Grosheva, I., Marthiens, V., Irinopoulou, T., Riou, J.-F., Bershadsky, A., and Mège, R.-M. (2004) Lamellipodium extension and cadherin adhesion: Two cell responses to cadherin activation relying on distinct signalling pathways. *J. Cell Sci.* **117,** 257–270
41. Ganz, A., Lambert, M., Saez, A., Silberzan, P., Buguin, A., Mège, R. M., and Ladoux, B. (2006) Traction forces exerted through N-cadherin contacts. *Biol. Cell* **98,** 721–730
42. Taus, T., Köcher, T., Pichler, P., Paschke, C., Schmidt, A., Henrich, C., and Mechtler, K. (2011) Universal and confident phosphorylation site localization using phosphoRS. *J. Proteome Res.* **10,** 5354–5362
43. Perez-Riverol, Y., Csordas, A., Bai, J., Bernal-Llinares, M., Hewapathirana, S., Kundu, D. J., Inuganti, A., Griss, J., Mayer, G., Eisenacher, M., Pérez, E., Uszkoreit, J., Pfeuffer, J., Sachsenberg, T., Yilmaz, S., Tiwary, S., Cox, J., Audain, E., Walzer, M., Jarnuczak, A. F., Ternent, T., Brazma, A., and Vizcaíno, J. A. (2019) The PRIDE database and related tools and resources in 2019: Improving support for quantification data. *Nucleic Acids Res.* **47,** D442–D450
44. Soper, D. S. (2019) Significance of the Difference between Two Slopes Calculator [Software]. Available from http://www.danielsoper.com/statcalc
45. Stelzer, G., Rosen, N., Plaschkes, I., Zimmerman, S., Twik, M., Fishilevich, S., Stein, T. I., Nudel, R., Lieder, I., Mazor, Y., Kaplan, S., Dahary, D., Warshawsky, D., Guan-Golan, Y., Kohn, A., Rappaport, N., Safran, M., and Lancet, D. (2016) The GeneCards Suite: From gene data mining to disease genome sequence analyses. *Curr. Protoc. Bioinformatics* **54,** 1.30.1–1.30.33
46. Subramanian, A., Tamayo, P., Mootha, V. K., Mukherjee, S., Ebert, B. L., Gillette, M. A., Paulovich, A., Pomeroy, S. L., Golub, T. R., Lander, E. S., and Mesirov, J. P. (2005) Gene set enrichment analysis: A knowledge-based approach for interpreting genome-wide expression profiles. *Proc. Natl. Acad. Sci. U.S.A.* **102,** 15545–15550
47. Mootha, V. K., Lindgren, C. M., Eriksson, K.-F., Subramanian, A., Sihag, S., Lehar, J., Puigserver, P., Carlsson, E., Ridderstråle, M., Laurila, E., Houstis, N., Daly, M. J., Patterson, N., Mesirov, J. P., Golub, T. R., Tamayo, P., Spiegelman, B., Lander, E. S., Hirschhorn, J. N., Altshuler, D., and Groop, L. C. (2003) PGC-1alpha-responsive genes involved in oxidative phosphorylation are coordinately downregulated in human diabetes. *Nat. Genet.* **34,** 267–273
48. Gao, F., Zhang, J., Wang, X., Yang, J., Chen, D., Huff, V., and Liu, Y.-X. (2014) Wt1 functions in ovarian follicle development by regulating granulosa cell differentiation. *Hum. Mol. Genet.* **23,** 333–341
49. Kusaka, M., Katoh-Fukui, Y., Ogawa, H., Miyabayashi, K., Baba, T., Shima, Y., Sugiyama, N., Sugimoto, Y., Okuno, Y., Kodama, R., Iizuka-Kogo, A., Senda, T., Sasaoka, T., Kitamura, K., Aizawa, S., and Morohashi, K. (2010) Abnormal epithelial cell polarity and ectopic epidermal growth factor receptor (EGFR) expression induced in Emx2 KO embryonic gonads. *Endocrinology* **151,** 5893–5904
50. Efimenko, E., Padua, M. B., Manuylov, N. L., Fox, S. C., Morse, D. A., and Tevosian, S. G. (2013) The transcription factor GATA4 is required for follicular development and normal ovarian function. *Dev. Biol.* **381,** 144–158
51. Tang, X., Xu, S., Li, R., Zhang, H., Chen, Q., Wu, W., and Liu, H. (2016) Polycomb repressive complex 1 (PRC1) regulates meiotic initiation of ovarian germ cells in chick embryos. *Mol. Cell. Endocrinol.* **437,** 171–182
52. Hu, X., Roberts, J. R., Apopa, P. L., Kan, Y. W., and Ma, Q. (2006) Accelerated ovarian failure induced by 4-vinyl cyclohexene diepoxide in Nrf2 null mice. *Mol. Cell. Biol.* **26,** 940–954
53. Le Masson, F., Razak, Z., Kaigo, M., Audouard, C., Charry, C., Cooke, H., Westwood, J. T., and Christians, E. S. (2011) Identification of heat shock factor 1 molecular and cellular targets during embryonic and adult female meiosis. *Mol. Cell. Biol.* **31,** 3410–3423
54. Tuna, M., Chavez-Reyes, A., and Tari, A. M. (2005) HER2/neu increases the expression of Wilms' tumor 1 (WT1) protein to stimulate S-phase proliferation and inhibit apoptosis in breast cancer cells. *Oncogene* **24,** 1648–1652
55. Fang, D., Hawke, D., Zheng, Y., Xia, Y., Meisenhelder, J., Nika, H., Mills, G. B., Kobayashi, R., Hunter, T., and Lu, Z. (2007) Phosphorylation of beta-catenin by AKT promotes beta-catenin transcriptional activity. *J. Biol. Chem.* **282,** 11221–11229
56. Robitaille, A. M., Christen, S., Shimobayashi, M., Cornu, M., Fava, L. L., Moes, S., Prescianotto-Baschong, C., Sauer, U., Jenoe, P., and Hall, M. N. (2013) Quantitative phosphoproteomics reveal mTORC1 activates de novo pyrimidine synthesis. *Science* **339,** 1320–1323
57. Inoki, K., Li, Y., Zhu, T., Wu, J., and Guan, K.-L. (2002) TSC2 is phosphorylated and inhibited by Akt and suppresses mTOR signalling. *Nat. Cell Biol.* **4,** 648–657
58. Sancak, Y., Thoreen, C. C., Peterson, T. R., Lindquist, R. A., Kang, S. A., Spooner, E., Carr, S. A., and Sabatini, D. M. (2007) PRAS40 is an insulin-regulated inhibitor of the mTORC1 protein kinase. *Mol. Cell* **25,** 903–915
59. Iadevaia, V., Liu, R., and Proud, C. G. (2014) mTORC1 signaling controls multiple steps in ribosome biogenesis. *Semin. Cell Dev. Biol.* **36,** 113–120
60. van Slegtenhorst, M., Nellist, M., Nagelkerken, B., Cheadle, J., Snell, R., van den Ouweland, A., Reuser, A., Sampson, J., Halley, D., and van der Sluijs, P. (1998) Interaction between hamartin and tuberin, the TSC1 and TSC2 gene products. *Hum. Mol. Genet.* **7,** 1053–1057
61. Li, Y., Inoki, K., Yeung, R., and Guan, K.-L. (2002) Regulation of TSC2 by 14–3-3 binding. *J. Biol. Chem.* **277,** 44593–44596
62. Plas, D. R., and Thompson, C. B. (2003) Akt activation promotes degradation of tuberin and FOXO3a via the proteasome. *J. Biol. Chem.* **278,** 12361–12366
63. Mueck, K., Rebholz, S., Harati, M. D., Rodemann, H. P., and Toulany, M. (2017) Akt1 stimulates homologous recombination repair of DNA double-strand breaks in a Rad51-dependent manner. *Int. J. Mol. Sci.* **18,** E2473
64. Irie, H. Y., Pearline, R. V., Grueneberg, D., Hsia, M., Ravichandran, P., Kothari, N., Natesan, S., and Brugge, J. S. (2005) Distinct roles of Akt1 and Akt2 in regulating cell migration and epithelial-mesenchymal transition. *J. Cell Biol.* **171,** 1023–1034
65. Liu, H., Radisky, D. C., Nelson, C. M., Zhang, H., Fata, J. E., Roth, R. A., and Bissell, M. J. (2006) Mechanism of Akt1 inhibition of breast cancer cell invasion reveals a protumorigenic role for TSC2. *Proc. Natl. Acad. Sci. U.S.A.* **103,** 4134–4139
66. Chin, Y. R., and Toker, A. (2009) Function of Akt/PKB signaling to cell motility, invasion and the tumor stroma in cancer. *Cell. Signal.* **21,** 470–476
67. Petrie, R. J., Doyle, A. D., and Yamada, K. M. (2009) Random versus directionally persistent cell migration. *Nat. Rev. Mol. Cell Biol.* **10,** 538–549
68. Chung, C. Y., Potikyan, G., and Firtel, R. A. (2001) Control of cell polarity and chemotaxis by Akt/PKB and PI3 kinase through the regulation of PAKa. *Mol. Cell* **7,** 937–947
69. Onishi, K., Higuchi, M., Asakura, T., Masuyama, N., and Gotoh, Y. (2007) The PI3K-Akt pathway promotes microtubule stabilization in migrating fibroblasts. *Genes Cells* **12,** 535–546
70. Ju, X., Katiyar, S., Wang, C., Liu, M., Jiao, X., Li, S., Zhou, J., Turner, J., Lisanti, M. P., Russell, R. G., Mueller, S. C., Ojeifo, J., Chen, W. S., Hay, N., and Pestell, R. G. (2007) Akt1 governs breast cancer progression in vivo. *Proc. Natl. Acad. Sci. U.S.A.* **104,** 7438–7443